Ocean oxygenation during the Middle Ordovician: links to biodiversification?

Senior Thesis
Submitted in partial fulfillment of the requirements for the
Bachelor of Science Degree
At The Ohio State University

By

Charles W. Diamond
The Ohio State University
2013

Approved by

Matthew R. Saltzman, Advisor
School of Earth Sciences

Table of Contents

Abstract

During the Ordovician period, biological diversity experienced a threefold increase (Great Ordovician Biodiversification Event). This expansion took place in several steps, with one of the largest pulses of diversification occurring in the Middle Ordovician (Darriwilian). This study presents paired carbon isotope data from carbonate and organic matter from the Antelope Valley Limestone of Meiklejohn Peak, Nevada, a Darriwilian carbonate sequence. A correlation is established between this section and two Estonian drill cores in which the MDICE has been previously reported. This correlation, based on carbon isotope stratigraphy, is supported by paleontological evidence. These data represent the first documentation of the Mid-Darriwilian Carbon Isotope Excursion (MDICE) from western Laurentia. The paired results of this study show a stepwise increase of approximately 3‰ in photosynthetic fractionation through the early stages of the MDICE, consistent with an increase in atmospheric oxygen of up to 18% (i.e. an increase from a starting atmospheric oxygen concentration of 10% to 28%). Increases in atmospheric oxygen are thought to have played a critical role in key evolutionary developments throughout time, such as the rise of animals at the end of the Precambrian and the gigantism seen in arthropods of the Permo-Carboniferous. The timing of the pulse of oxygen observed in the Darriwilian coincides with the timing of rapid biodiversification, suggesting that the two may have been intimately linked.

1. Introduction

The oldest greenhouse to icehouse transition of the Phanerozoic Eon took place during the Ordovician period, although the precise timing of this climate transition and links to the evolution of life remain poorly known. The Early Ordovician was characterized by a hot-house climate and low levels of biodiversity (Trotter et al., 2008). By the Middle Ordovician, a sustained cooling trend had taken equatorial sea surface temperatures into the modern day range (Trotter et al., 2008). During this epoch, the biosphere experienced the most rapid and dramatic expansion in diversity of the Phanerozoic (Sepkoski, 1995). Throughout the whole of the Ordovician, biodiversity saw a threefold increase, an event known as the Great Ordovician Biodiversification Event or GOBE (Sepkoski, 1995). The causes of the diversification and radiation are not well understood. There were many geologic processes taking place coincidently which may have contributed. Among them were the flooding of large, low lying, sections of the continents and high rates of volcanism and tectonism. There were several sizable transgressive events during the early Darriwilian, followed by a large transgression in the middle Darriwilian that began the Late Llanvirn-Caradoc Highstand (Nielsen, 2004). The heightened magmatic activity of the Middle Ordovician is evident in the deposition of the largest betonites seen in the Phanerozoic, as well as in a steep shift in the $^{87}Sr/^{86}Sr$ of seawater toward less radiogenic values (Young et al., 2009). The Taconic Orogeny was also beginning at this time.

One factor that has been suggested to play a key role in periods of origination and evolution, but has received relatively little attention for the GOBE interval, is

atmospheric oxygen concentration (Berner et al., 2007). Examples of the connection between oxygenation and evolution are the rise of animals in the latest Precambrian (Canfield et al., 2007) and the gigantism seen in arthropods of the Permo-Carboniferous (Graham et al, 1995; Dudley, 1998). Few proxies exist for atmospheric O_2%, however, ε_p (the ability of photosynthetic life to fractionate light carbon from $CO_{2(aq)}$) has been shown to increase with increasing atmospheric pO_2 (Berner et al, 2000). Thus, the difference between the carbon isotopic composition of sedimentary organic matter ($\delta^{13}C_{org}$) and that of the carbonate rocks encapsulating it ($\delta^{13}C_{carb}$) could serve as an indicator of changing oxygen levels (Saltzman et al, 2011). Herein this difference ($\delta^{13}C_{carb}$ - $\delta^{13}C_{org}$) will be referred to as $\Delta^{13}C$.

In this study, I present paired $\delta^{13}C_{carb}$ and $\delta^{13}C_{org}$ data from a Darriwilian carbonate succession at Meiklejohn Peak, Nevada. The biostratigraphy for this section is constrained by the presence of conodont index species of both the North Atlantic and North American Midcontinent conodont zonation systems (Harris et al., 1977). In addition, the presence of the globally recognized Mid-Darriwilian $\delta^{13}C_{carb}$ Excursion (MDICE) serves as an important temporal marker (Ainsaar et al., 2010). These correlation tools together indicate that my section records Stage Slice Dw2 , during which large pulses of biodiversification took place (Fig. 1) (Bergström et al., 2009; Webby et al., 2004). My results show that $\Delta^{13}C$ and oxygen levels increased during the Dw2 Stage Slice, consistent with a role in biodiversification.

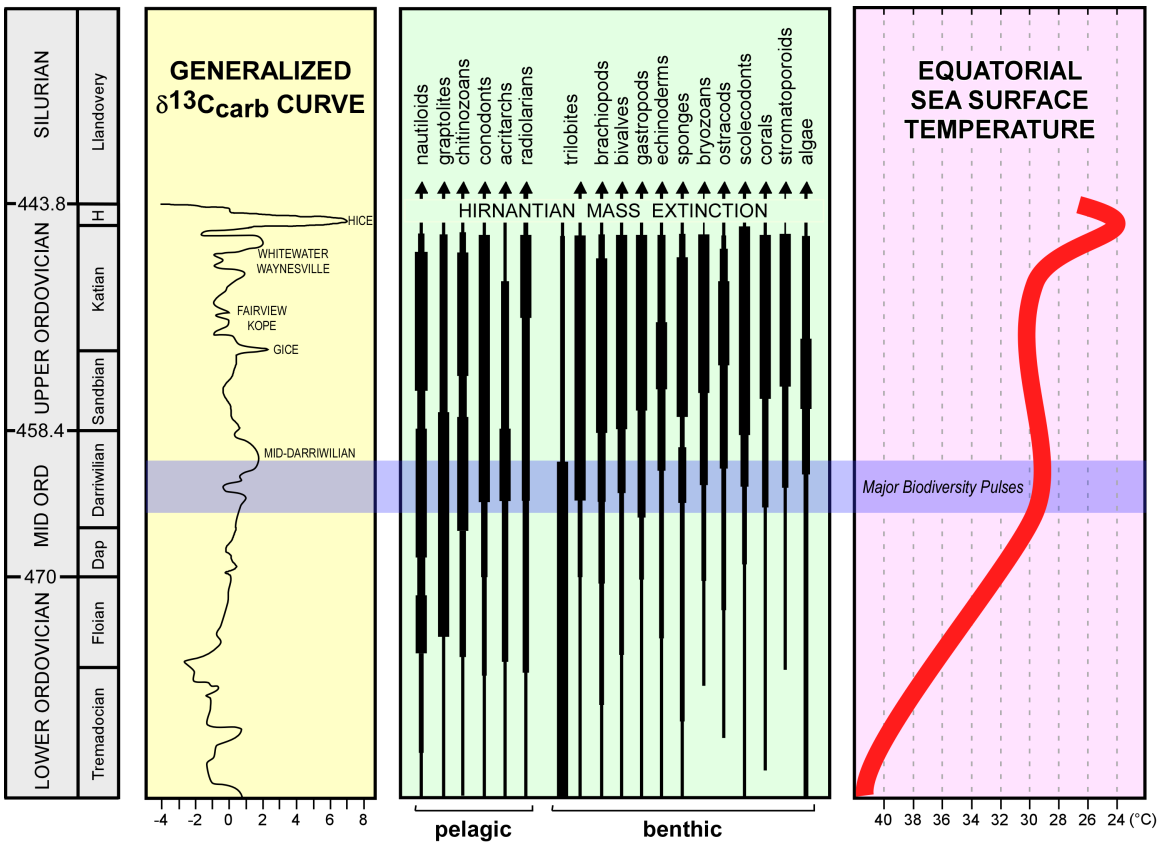

Figure 1. Left panel, the Ordovician timescale (Cooper and Sadler, 2012). Left center panel, generalized composite $\delta^{13}C_{carb}$ curve for the Ordovician (modified from Bergström et al., 2009). Right center panel, diversity trends for major faunal groups of the Ordovician. Thickening of lines indicates biodiversification pulses and is not proportional between groups (figure modified from Trotter et al., 2008; data compiled from Webby et al., 2004). Right panel, sea surface temperature curve for the Ordovician (modified from Trotter et al., 2008)

2. Background

2.1 Geologic setting

During the Middle Ordovician, Laurentia was drifting northward, roughly centered on the equator (Fig. 2) (Cocks and Torsvik, 2002). Portions of the Gondwana supercontinent (i.e. Australia, Antarctica, and India), Baltica, Siberia, and South China were also near the intertropical convergence zone (Cocks and Torsvik, 2002). Sea level was substantially higher than the present day, leaving large portions of the continents flooded with shallow epeiric seas (Nielsen, 2004; Haq and Schutter, 2008). Thick successions of carbonates were deposited through the Early and Middle Ordovician along the western margin of Laurentia in an extensive platform/ramp environment (Ross et al., 1989; Miller et al., 2012). Relatively continuous carbonate deposition was interrupted by the Eureka Quartzite, a regionally diachronous Middle and Upper Ordovician clastic formation (Harris et al., 1977). The Neogene extensional tectonics that created the Basin and Range province of western North America exposed many sections of Ordovician carbonate. Among these is the exposure found at Meiklejohn Peak, Nevada.

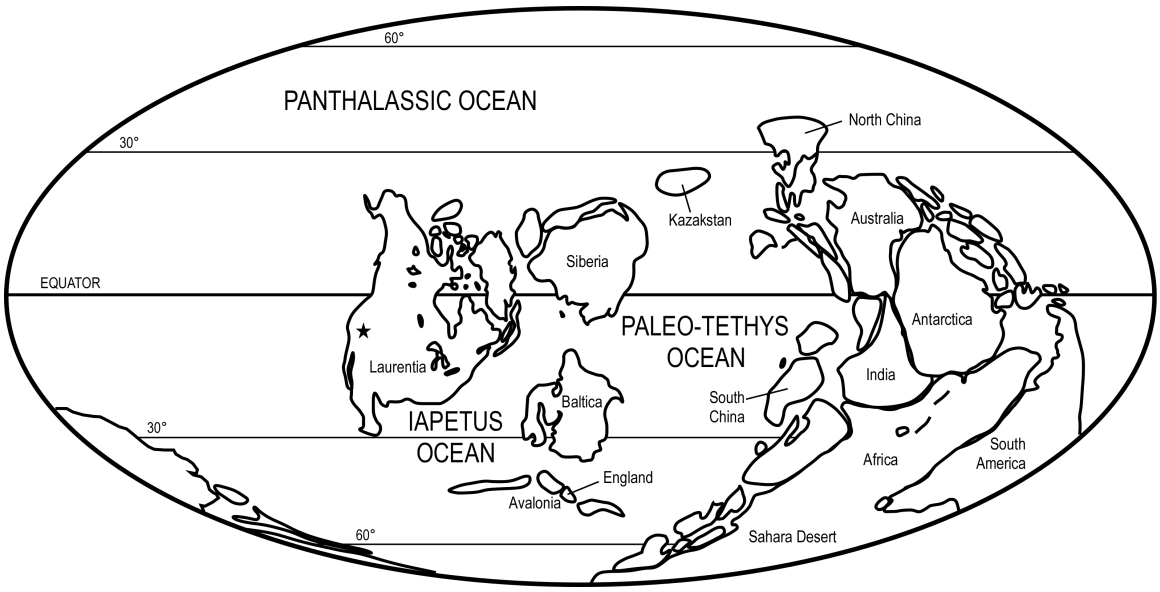

Figure 2. Middle Ordovician paleogeographic map showing the positions of the continents (after Cocks and Torsvik, 2002), star indicates the location of Meiklejohn Peak.

2.2 Meiklejohn Peak, Nevada

Meiklejohn Peak is situated in the northeast corner of the Bare Mountain Quadrangle of southwestern Nevada. There are exposures of Ordovician limestones and calcareous shales along its west flank with a high angle fault dividing the northwest slope from the southwest. The south fault block has been uplifted relative to the north. On both the northwest and southwest sides of Meiklejohn, the top of the Goodwin Limestone, the Nine Mile Shale, and part of the Antelope Valley Limestone are exposed, and moving to the north, the entire Antelope Valley Limestone is exposed along with the overlying Eureka Quartzite and Ely Springs Dolomite (Fig. 3). The line of section sampled follows Harris et al. (1979) and is indicated by the red dashed line in Figure 3.

The section begins just below the informal middle member of the Antelope Valley Limestone and continues up to the base of the Eureka, sampling at a 1.5m interval.

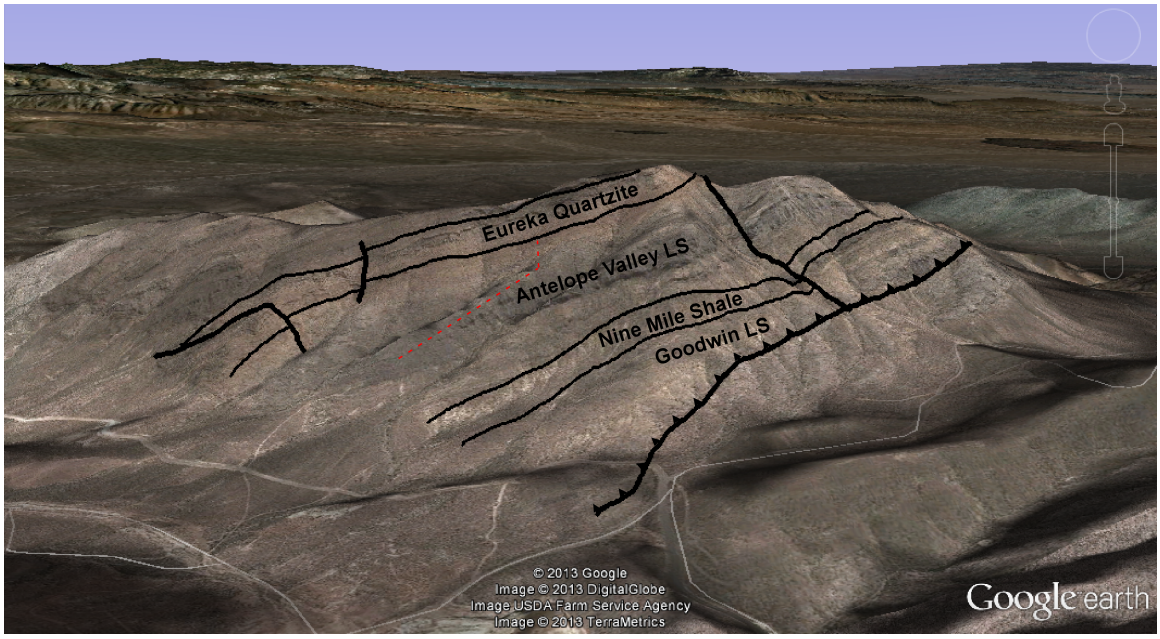

Figure 3. View of Meiklejohn Peak from the west showing formation contacts and major faults. The thickened toothed line indicates the position of the bounding thrust fault (after Monsen et al., 1992)

2.3 Lithology

The Antelope Valley Limestone is divided into three informal members (Ross et al., 1972). The lower member is characterized generally as micrites to wackestones with some coarse packstone beds throughout. A large biohermal mound on the southwest slope, away from my line of section, has been the focus of extensive study (e.g., Ross, 1972; Krause and Rowell, 1975). I estimate that 13 m of the uppermost lower member were sampled in my section. The lower-middle member contact is defined by medium grey, oscillating wackestones and micrites of the lower member below (Fig. 4 panel A) and the first occurrence of massively bedded, light grey, nodular packstone of the middle member above (Fig. 4 panel B).

The middle member is approximately 90 m thick and is almost entirely composed of massive, often oncolitic, packstones. The middle 50 m is at times heavily burrowed, with burrows being silty and weathering to an orange brown. Resistant, 1 m, oncolitic beds are present at 51 m and 57 m in my measured section and thicker, 2-3 m, oncolitic beds occur at 75 m and 98 m. The middle-upper member contact is at 102 m as defined by the last occurrence of a massive, light grey packstone of the middle member below and a transition into silty, thinner bedded, darker lime mudstone of the upper member above.

The upper member of the Antelope Valley Limestone is approximately 170 m thick and is composed mainly of thinner bedded, homogeneous, dark grey micrite (Fig 4 panel E). Several intervals contain thin silty micrite beds interbedded cyclically with cleaner micrites forming “ribbon” limestone. At 150 m in my section there is a more resistant interval, toward the top of which there is a succession of repeated, 2 m cycles of

unbioturbated ribbon limestone, heavily bioturbated wackestone, and then massive packstone. This is followed by homogenous, dark grey micrite until the top of the section where, approximately 20m below the base of the overlying Eureka, the rocks become coarser, with interbedded clastic material. Nearing the Eureka, the fossiliferous packstones become increasingly sandy. The Eureka-Antelope Valley Limestone contact is defined by the last occurrence of medium to dark grey packstone of the Antelope Valley Limestone below the contact, and above it, a thick, massive, cliff forming, buff orange quartzite of the Eureka Quartzite.

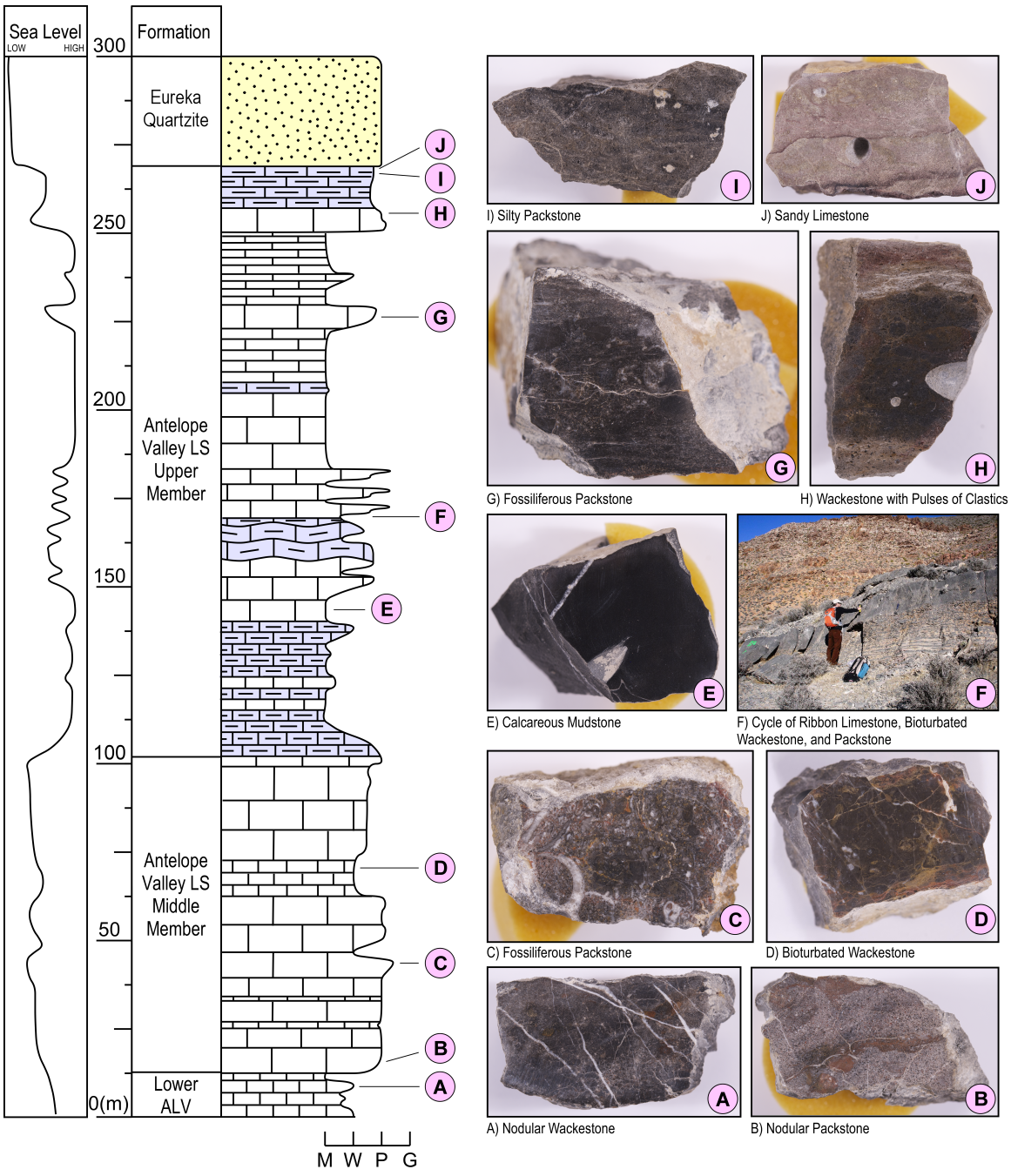

Figure 4. Stratigraphic column from Meiklejohn Peak showing interpreted local relative sea level and photographs of polished surfaces of selected key lithologies. Panel F shows one of several meter scale cycles repeated through an interval of the upper member.

2.4 Biostratigraphy

A fairly comprehensive biostratigraphic framework has been established for the Ordovician (Bergström, 1986; Cooper and Sadler, 2012). The most useful fossils for correlation in the Ordovician are graptolites and conodonts, with graptolites being found mainly in shales deposited in slope environments and conodonts primarily being found in shallower platform and ramp carbonate deposits. Meiklejohn Peak is somewhat unique in that it contains both North Atlantic and North American Midcontinent conodont species (Harris et al., 1979).

Several species collected from Meiklejohn Peak are useful for global correlation, namely Midcontinent species *H. holodentata, P. polonicus,* and *C. sweeti* and North Atlantic species *E. suecicus* and *B. gerdae* (Harris et al., 1979). The *H. holodentata* zone is the oldest present and is contemporaneous with the North Atlantic *E. variabilis* zone. The *P. polonicus* and *E. suecicus* zones follow them, with the *P. polonicus zone* extending slightly further. Above these, several zones are not represented by zonal index fossils in this section, namely the Midcontinent *C. friendsvillensis* zone and the North Atlantic *P. serra* and *P. anserinus* zones. Approximately 10m above the last collection of *P. polonicus*, *C. sweeti* was collected, and *B. gerdae* (a member of the *A. tvaerensis* group) was collected 9m above that (Harris et al., 1977). The space between the top of the *P. polonicus* zone and the bottom of the *B. gerdae* zone represents approximately 6 million years (Cooper and Sadler, 2012). This indicates that the top of the section at Meiklejohn Peak is quite condensed.

2.5 $\Delta^{13}C$

$\Delta^{13}C$ represents the absolute difference between carbonates that are being precipitated and the organic matter that is contemporaneously being produced in the same ocean water. There are several factors that contribute to this difference other than ε_p (the photosynthetic fractionation effect) and consequently other mechanisms that can force changes in $\Delta^{13}C$. These factors include the temperature-dependent fractionation between DIC and $CO_{2(aq)}$, the primary carbonate mineral being precipitated (e.g. calcite vs. aragonite), and the possibility of a secondary fractionation being imparted on the sedimentary organic matter by heterotrophic organisms (Hayes et al., 1999). Increases in atmospheric O_2 have been shown to increase ε_p in both phytoplankton and vascular plants (Berner et al., 2000; Beerling et al., 2002). However, ε_p has also been demonstrated to be largely dependent upon pCO_2, scaling directly with the size of the CO_2 reservoir (Kump and Arthur, 1999). Consideration of these factors is therefore critical to any interpretation of $\Delta^{13}C$.

3. Methods

Carbonate samples were taken from a 270 m exposure of the Antelope Valley Limestone of Meiklejohn Peak at 1.5 m intervals. These samples were then drilled, avoiding veins, spar, and obvious burrows, to obtain 1-2 g of powder from each sample for carbon isotopic analysis. A small fraction of the powder was then analyzed for the carbon and oxygen isotopic compositions of carbonate at either the Ohio State University Stable Isotope Biogeochemistry Lab or the Indiana University Biogeochemistry Lab. At Ohio State, carbonate samples were processed using a Kiel III carbonate device directly

coupled to the inlet of a Finnigan Delta Plus VI gas source mass spectrometer to measure the $\delta^{13}C$ and $\delta^{18}O$ of the resultant, purged, CO_2. At Indiana University, carbonate samples were processed using a Gas Bench, directly coupled to the inlet of a Finnigan Delta Plus XP gas source mass spectrometer to analyze $\delta^{13}C$ and $\delta^{18}O$. The average reproducibility of repeated analyses was ± 0.082‰. Results are reported in per mil notation relative to the Vienna Peedee Belemnite.

For the analysis of organic carbon, 1-2 g of powder from each sample to be analyzed was acidified repeatedly using 6N HCl to remove any carbonate minerals. The samples were then rinsed 3 times with ultrapure water and dried for 24-48 hours at 75 °C. The residual insoluble material was homogenized and a small fraction was combusted using a Costech Elemental Analyzer. The $\delta^{13}C$ of the CO_2 gas emitted was measured using a Finnigan Delta Plus IV via a CONFLO III open-split interface. Sample processing and analysis was done at Ohio State. The average reproducibility for repeated analyses was ± 0.053‰. Results are, again, reported in ‰VPDB.

4. Results

4.1 $\delta^{13}C_{carb}$

79 samples were analyzed for the carbon and oxygen isotopic compositions of carbonate (Fig. 5). The $\delta^{13}C_{carb}$ results show a range in values from -2.73‰ to 0.79‰. There are several discernable trends in the data. The first 85m of my section show a steady negative trend beginning at values just below 0‰ and reaching -2.36‰ at 82.5 m. This is followed by rapid rise that exceeds the heaviest values near the bottom of the section, reaching values around 0.4‰. Both the negative trend and the subsequent rise to

positive values are contained within the Antelope Valley middle member. The positive trend peaks very near to the middle-upper member contact. Positive values are then sustained through the next 135 m of the upper member before dropping sharply in the uppermost 30 m. A sustained interval with steady positive $\delta^{13}C_{carb}$ values becomes more scattered near the start of the drop. The $\delta^{13}C_{carb}$ drop near the top of the section reaches the lightest values observed at -2.73‰.

4.2 $\delta^{18}O_{carb}$

The $\delta^{18}O$ data show a consistent positive linear trend from values around -7‰ to -8.5‰ at the bottom of the section, reaching the heaviest values of approximately -6‰ at the top of the micritic interval of the upper member. Above these heaviest values, in the very uppermost part of the section, the values are lighter and more scattered. This could be the result of meteoric fluids having migrated through the sediments during the regression that brought with it the deposition of the Eureka. The general trend in this section fits with the -5‰ to -8‰ range previously reported for the Middle Ordovician and agrees with a generally positive trend, toward heavier values, that has been reported throughout the Ordovician (Trotter et al., 2008).

In general, samples that produced lighter than expected $\delta^{18}O_{carb}$ values have $\delta^{13}C_{carb}$ values that fit the overall trend of the data. In accordance with this, it does not appear that diagenetic alteration significantly overprinted the values observed in $\delta^{13}C_{carb}$.

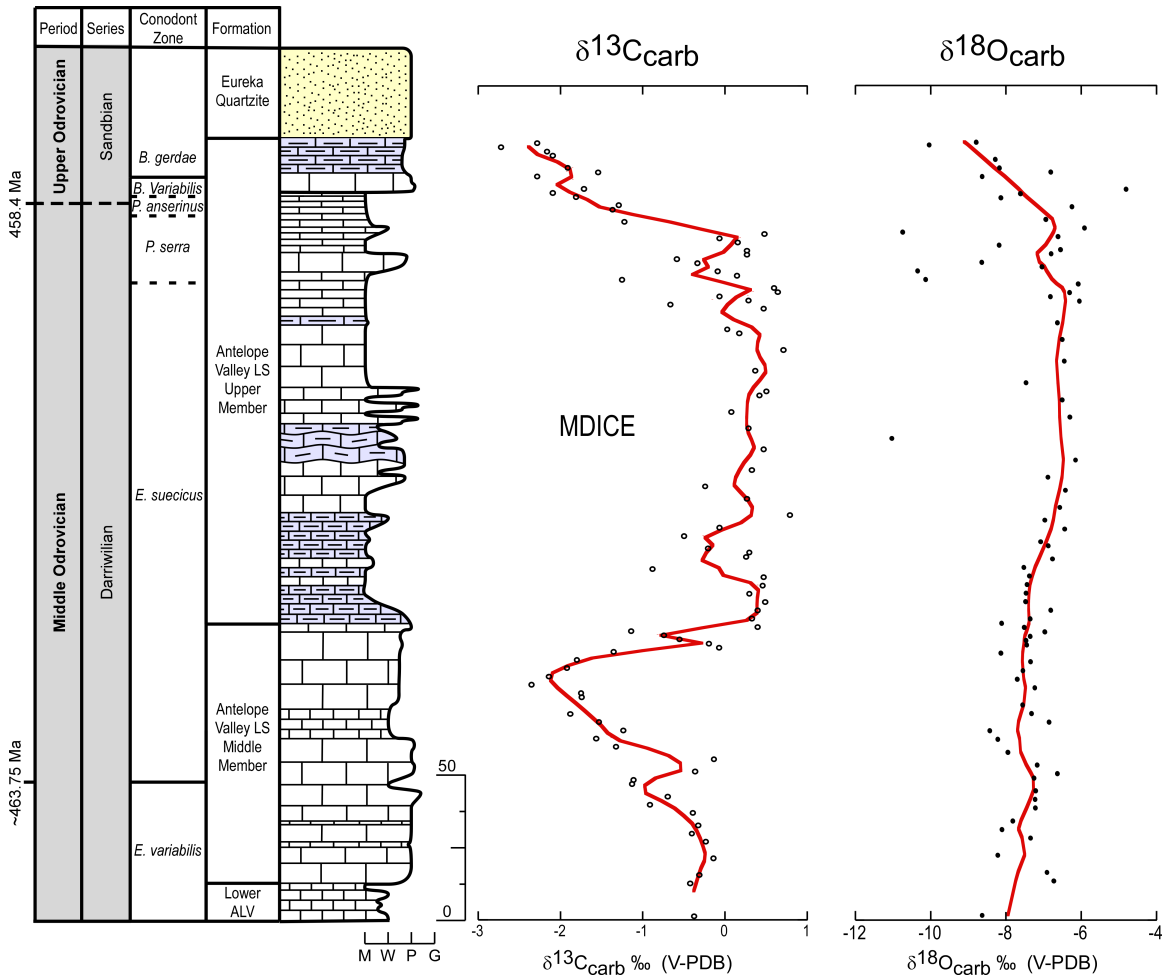

Figure 5. Stratigraphic column from Meiklejohn Peak with conodont zones and inferred chronostratigraphy along with $\delta^{13}C_{carb}$ and $\delta^{18}O_{carb}$ data. Best fit lines are 3-pt moving average for $\delta^{13}C_{carb}$ and 15% weighted best fit for $\delta^{18}O_{carb}$.

4.3 $\delta^{13}C_{org}$

41 samples were analyzed for the carbon isotopic compositions of the sedimentary organic matter (total organic carbon, TOC) contained within them (all of which were also analyzed for $\delta^{13}C_{carb}$). The $\delta^{13}C_{org}$ data ranges in values from -31.67‰ to -27.68‰ (Fig. 6). The data show a negative trend through the middle member, starting around -29‰ at the base of the section and falling ~2‰ to around -31‰ at the base of the upper member. Through the sustained positive interval of the broad MDICE peak, the values show a slight positive trend of ~1‰. In the upper 25m of my section, $\delta^{13}C_{org}$ rises abruptly from around -30‰ to -28‰. Evidence from conodont biostratigraphy indicates that this is a very condensed interval (Harris et al., 1979).

The negative trend of the middle member begins by roughly tracking the negative trend of $\delta^{13}C_{carb}$. It continues to trend negatively until it reaches relative stasis at the middle-upper member boundary (i.e. trending continuously through the rising limb of the MDICE). The $\delta^{13}C_{org}$ initially tracks $\delta^{13}C_{carb}$, but then deviates from this trend, steadily increasing the magnitude of difference between the two during the rising limb of the MDICE.

4.4 $\Delta^{13}C$

$\Delta^{13}C$ represents the difference between the carbon isotopic compositions of contemporaneously deposited carbonate and organic matter ($\delta^{13}C_{carb}$ - $\delta^{13}C_{org}$). The data from my section shows $\Delta^{13}C$ remaining relatively constant (perhaps showing a gradual decreasing trend) between 28‰ and 29‰ as $\delta^{13}C_{org}$ tracks $\delta^{13}C_{carb}$ through the majority of the middle member. As $\delta^{13}C_{carb}$ rises into the MDICE, near the middle-upper member

transition, $\delta^{13}C_{org}$ continues to trend toward lighter values, producing a stepwise jump in $\Delta^{13}C$ from ~28‰ to ~31‰. $\Delta^{13}C$ then shows a gradual negative trend through the broad MDICE peak as $\delta^{13}C_{carb}$ remains more or less constant and $\delta^{13}C_{org}$ slowly increases by ~1‰. At the top of the section, $\Delta^{13}C$ drops sharply from ~30‰ to ~25‰. This drop is produced by $\delta^{13}C_{carb}$ falling by ~2.5‰ to lighter values as $\delta^{13}C_{org}$ simultaneously becomes heavier by a similar amount.

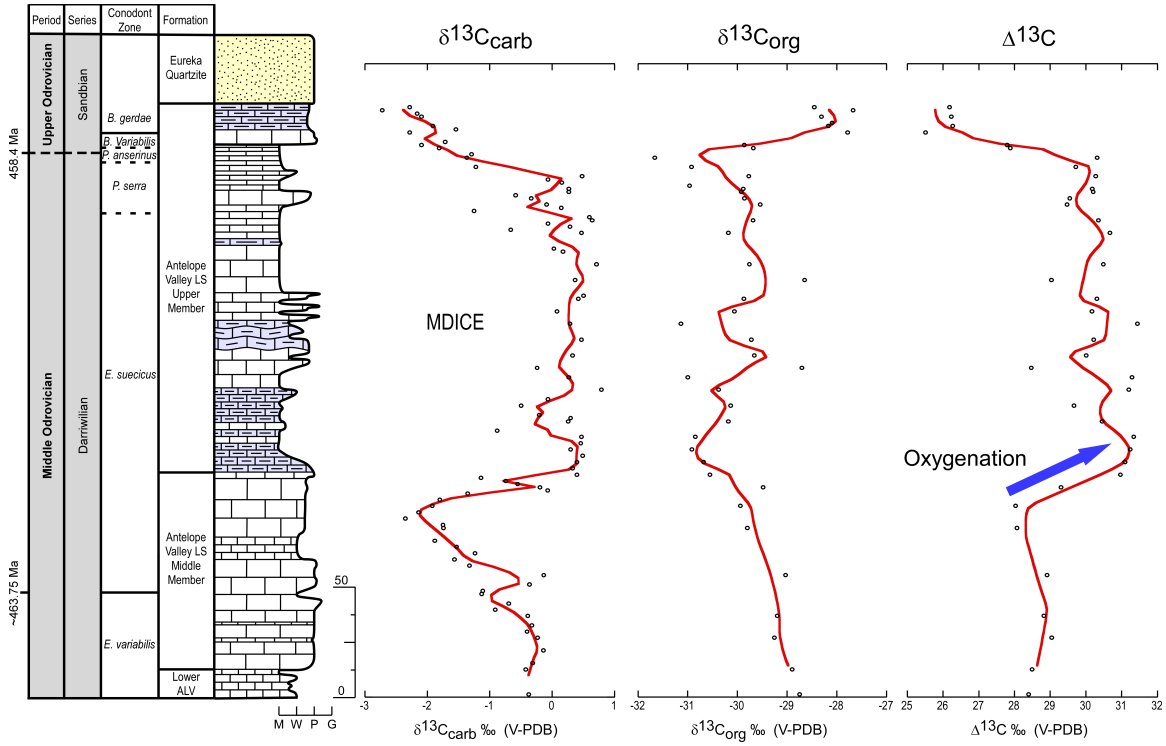

Figure 6. Stratigraphic column, conodont zonation and inferred chronostratigraphy from Meiklejohn Peak with $\delta^{13}C_{carb,}$ $\delta^{13}C_{org}$, and $\Delta^{13}C$ data.

5. Discussion

5.1 Correlation to Estonia

A thick and relatively continuous Ordovician carbonate succession can also be found in the subsurface of Estonia, having been deposited in a shallow ramp setting (Dronov and Rozhnov, 2007) on the eastern side of the Iapetus Ocean (Cocks and Torsvik, 2002). Several Estonian drill cores have been analyzed for $\delta^{13}C_{carb}$ and the MDICE excursion has been well documented in the Darriwilian sections (Ainsaar et al., 2004; Kaljo et al., 2007). The $\delta^{13}C_{carb}$ profile from Meiklejohn Peak is consistent with the $\delta^{13}C_{carb}$ trends that have been observed in these cores (Ainsaar et al., 2004; Kaljo et al., 2007) and agrees with the chemostratigraphic framework proposed in Ainsaar et al. (2010) for this time interval (Fig. 7).

Ainsaar et al. (2010) divided the MDICE excursion, as observed in several Balto-Scandian sections, into 5 intervals (i.e. BC1-5). Zone BC1 corresponds to the pre excursion interval. The top of BC1 is defined by the isotopically lightest value in the pre MDICE negative shift. Zone BC2 is then the rising limb of the MDICE. In multiple Estonian sections, a very short-lived negative step is present in this rise. This step is also seen in the data presented here. The broad peak of the MDICE defines the BC3 zone. BC4 is the falling limb, returning to or exceeding the lightest value seen at the BC1-BC2 zonal boundary. BC5 is the post excursion interval, which is not captured by the Meiklejohn section. Rather, The Eureka Quartzite truncates the upper BC4 interval.

Conodont biostratigraphy also supports the correlation of this section to the Estonian intervals containing the MDICE (Mannik and Viira, 2005; Viira et al., 2006; Bergström, 2007; Schmitz et al., 2010). The Kerguta 565 and Mehikoorma 421 drill

cores contain the conodonts *E. suecicus* and *E. variabilis* (Viira et al., 2006; Mannik and Viira, 2005). The stratigraphic positions of these index fossils relative to the contours of the $\delta^{13}C_{carb}$ chemostratigraphy agree with what has been observed at Meiklejohn Peak (Fig 5) (Harris et al, 1979; this study).

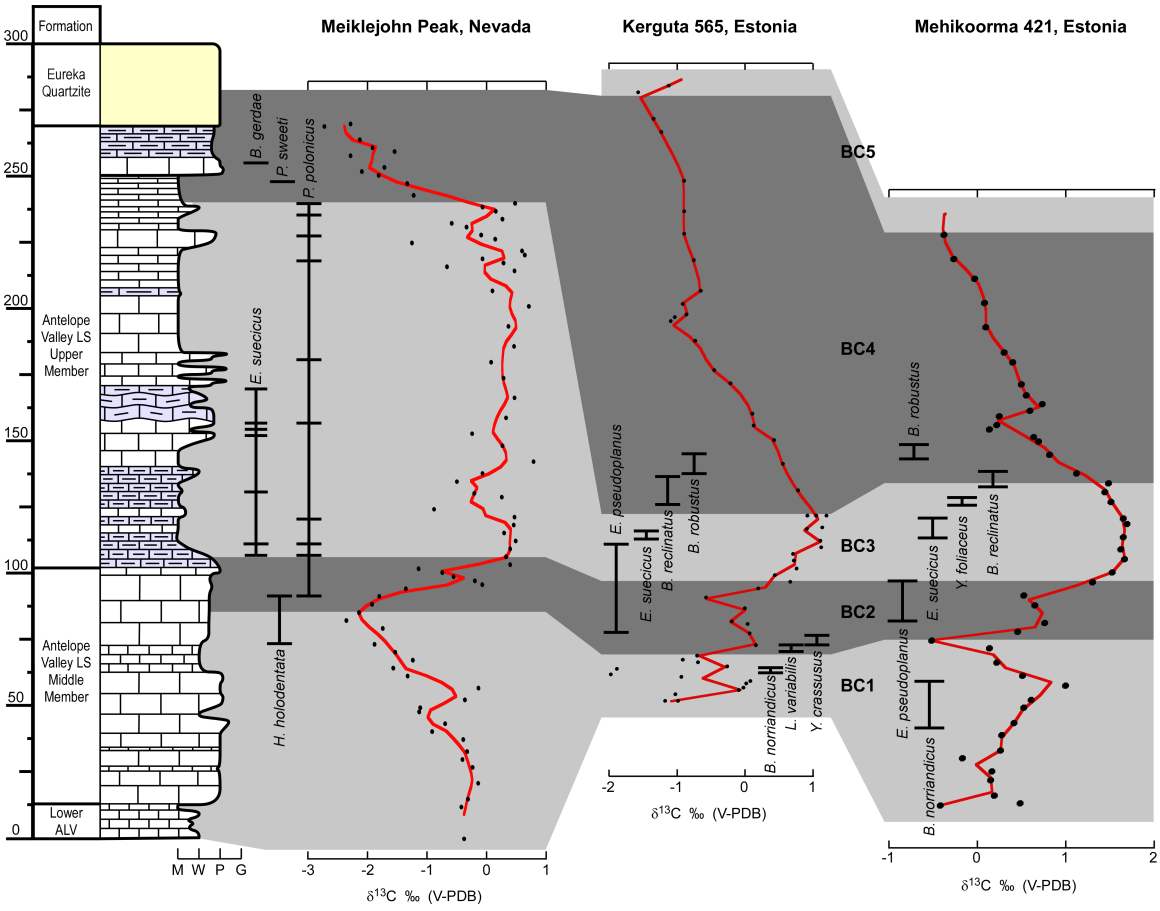

Figure 7. Stratigraphic column, conodont ranges (Harris et al., 1977), and $\delta^{13}C_{carb}$ data from Meiklejohn Peak correlated to sections of the Kerguta and Mehikoorma Estonian cores using the chemostratigraphic zones of Ainsaar et al., 2010. Estonian data and conodont ranges replotted from Ainsaar et al., 2010.

5.2 Interpretation of $\delta^{13}C_{carb}$

The rising limb of the MDICE occurs in close proximity to the middle-upper member boundary of the Antelope Valley Limestone at Meiklejohn Peak, which represents a transition from coarse wackestone/packstone to fine grained, homogeneous lime muds. I interpret this lithological change to signify a transgressive event. A fining in grain size is also evident in the early MDICE of a section in Maryland (Saltzman et al., in prep.), supporting the idea that this apparent deepening signifies a global eustatic transgression. The Ordovician sea level curve of Nielsen (2004) also shows a transgression near the base of the *E. suecicus* and *P. polonicus* zones, further supporting this notion.

This transgression would have significantly increased the burial flux of organic carbon. Organic matter is primarily buried in deltaic and shelf environments (Berner, 2004), which increase in abundance during a transgression. Increasing the total flux of organic matter into the rock reservoir would have exported large amounts of light carbon from the ocean, driving the carbon isotopic composition of seawater to heavier values, providing a possible mechanism for producing the MDICE excursion.

Photosynthesis also releases oxygen. By burying the organic matter before aerobic bacteria have a chance to break it down, a net gain in the O_2 content of the ocean-atmosphere system is achieved. Therefore, by increasing the organic burial flux, a coeval rise in the carbon isotopic composition of seawater and in the oxygen content of the ocean was produced. The mechanism for the eustatic rise remains unclear, however, an increase in sea-floor spreading rates could provide such a mechanism.

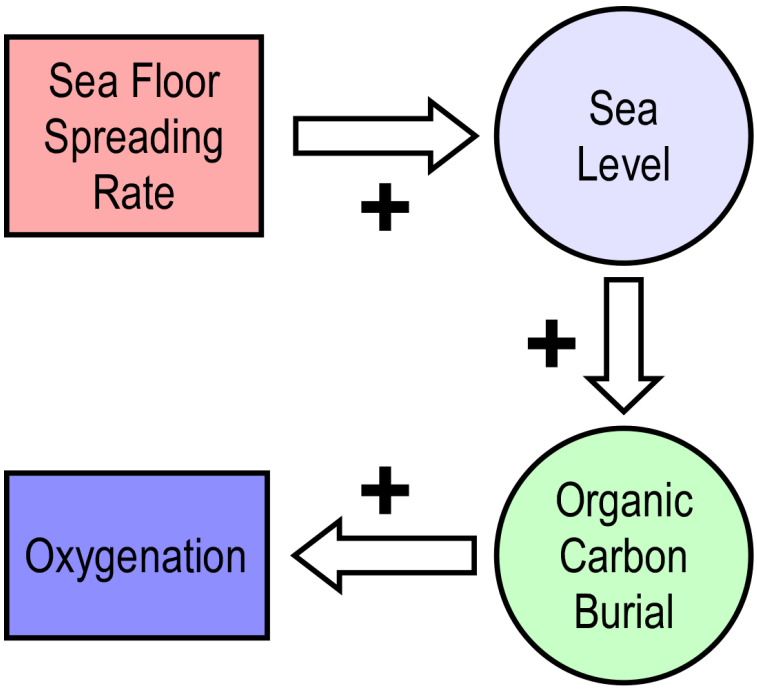

Figure 8. System diagram showing possible mechanism for oxygenation.

5.3 Interpretation of $\Delta^{13}C$

As $\delta^{13}C_{carb}$ is rising into the MDICE interval, I have shown that $\Delta^{13}C$ experienced a stepwise increase of ~3‰. The interpretation that the driving force behind this change was an increase in ε_p is supported by the coincidence with an interval of steady temperature as demonstrated by $\delta^{18}O_{apatite}$ of conodont elements (Trotter et al., 2008), and a lack of evidence for a change in carbonate mineralization. ε_p has been demonstrated to scale with multiple factors. pCO_2 has been demonstrated as a first order control on ε_p and as such, $\Delta^{13}C$ has been used in multiple studies as a proxy for atmospheric CO_2 level (e.g., Kump et al., 1999; Joachimski et al., 2002). The interpretation that the change in $\Delta^{13}C$ observed in this data was caused by a change in pCO_2, however, would be

inconsistent with the contemporaneous rise in the paired $\delta^{13}C_{carb}$ data, which I interpret as an interval of increased organic burial. Changes in pO_2 have also been shown to have a first order effect on ε_p in both marine plankton and vascular plants (Berner et al., 2000; Beerling et al., 2002). This is because pCO_2 rises within a cell as photorespiration increases because O_2 can outcompete CO_2 for sites on the photosynthetic enzyme Rubisco.

ε_p can also change with changes in a phytoplankton's growth rate or surface to volume ratio (Popp et al., 1998; Hayes et al., 1999; Joachimski et al., 2002). The possibility that this factor affected the rise in $\Delta^{13}C$ seen in the early MDICE exists. However, it is a more parsimonious interpretation that this rise was caused by an increase in atmospheric pO_2, given the apparent coeval rise in organic carbon burial. Using the data from Berner et al. (2000) as a template and an assumed starting atmospheric O_2 of 10%, the rise in $\Delta^{13}C$ of ~3‰ corresponds to an increase in O_2 of 18% (Fig. 9).

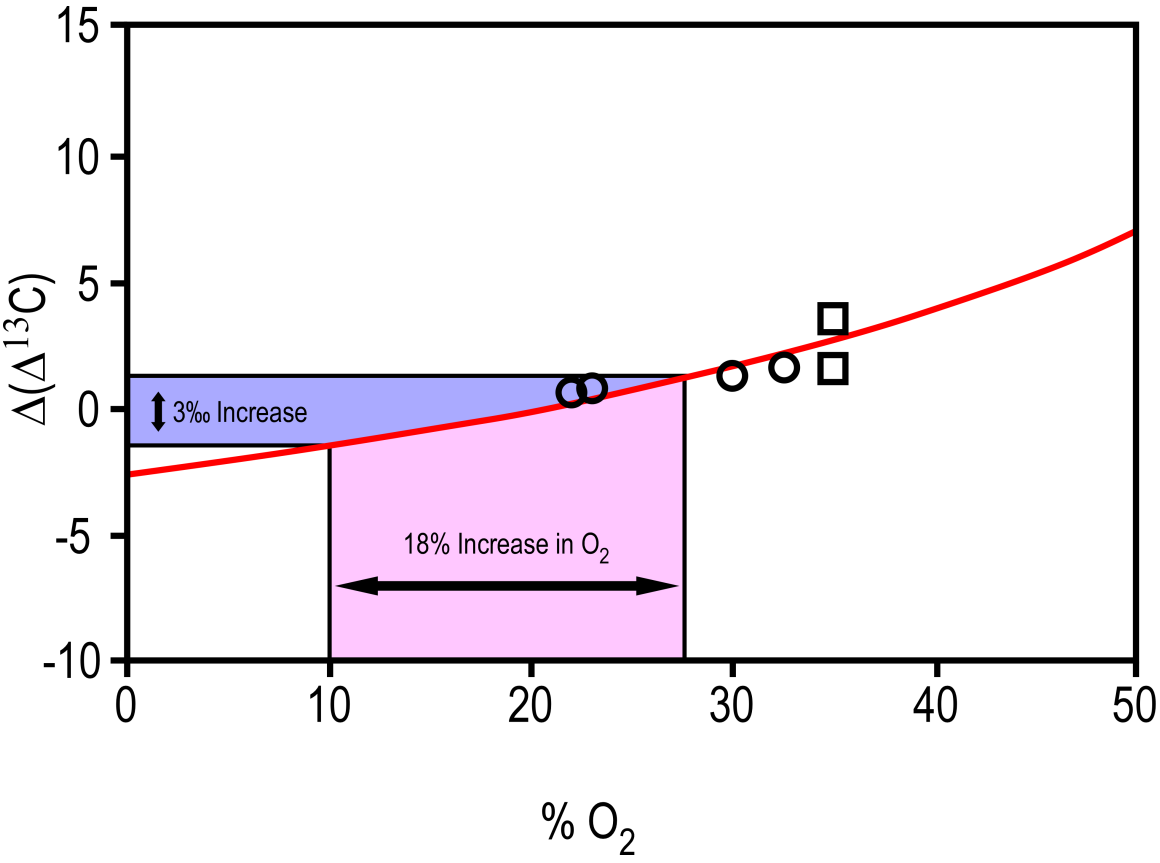

Figure 9. Plot showing experimental data from Berner et al., 2000 and the approximate increase in $\%O_2$ required to produce a 3‰ increase in $\Delta^{13}C$.

5.4 Conclusions

The paired $\delta^{13}C_{carb}$ and $\delta^{13}C_{org}$ data presented here represent the first demonstration of the MDICE in western Laurentia and the first $\delta^{13}C_{org}$ data to be obtained for this interval of time. The rising limb of the MDICE excursion takes place during Stage Slice Dw2 (Bergström et al., 2009), which is a critically important interval of time as it coincides with one of the largest pulses of biodiversification observed in the GOBE (Webby et al., 2004). The evidence presented here has demonstrated that this rise in the carbon isotopic composition of seawater was coupled to a rise in atmospheric oxygen of as much as 18% through the shared mechanism of enhanced organic carbon burial. Given the evidence for a connection between oxygenation and evolution at other time in the geologic past, the idea that oxygen played a key role in this pulse of the GOBE certainly holds promise.

5.5 Future work

To further constrain the magnitude of this increase in oxygen, future work should include measurement of $\delta^{13}C_{org}$ in other locations. Sulfur isotope and trace metal analysis and of this section, as well as other locations, would also aid in building a more comprehensive view of the oxygen mass-balance and redox state of this critical time in Earth's history.

Acknowledgements

The Stable Isotope Lab at Ohio State (Andréa Grottoli and Yohei Matsui) and the Biogeochemistry Lab at Indiana University are gratefully acknowledged for analysis of samples. I would like to thank Cody Trigg for help with fieldwork and sample preparation, Cole Edwards for help with lab procedures, fieldwork, sample preparation, helpful discussion and for delivering samples to Indiana University, and Alexa Sedlacek for helpful discussion. I would also like to thank Jen Foren for help with photography and for supporting me through the many sleepless nights spent working on this project and others. I would like to express my deepest gratitude to Matt Saltzman for his guidance and persistent support throughout the past year, as well as for giving me the opportunity to make this project my own.

References

Ainsaar, L., Meidla, T., Tinn, O., 2004, Middle and Upper Ordovician stable isotope stratigraphy across the facies belte in the East Baltic: Conference materials, Tartu University Press, Tartu, p. 11-12

Ainsaar, L., Kaljo, D., Martma, T., Meidla, T., Mannik, P., Nolvak, J., Tinn, O., and Early Palaeozoic palaeoenvironments, 2010, Middle and Upper Ordovician carbon isotope chemostratigraphy in Baltoscandia: A correlation standard and clues to environmental history: Palaeogeography, Palaeoclimatology, Palaeoecology, v. 294, p. 189-201.

Beerling, D.J., Lake, J.A., Berner, R.A., Hickey, L.J., Taylor, D.W., and Royer, D.L., 2002, Carbon isotope evidence implying high O_2/CO_2 ratios in the Permo-Carboniferous atmosphere: Geochimica Et Cosmochimica Acta., v. 66, p. 3757-3767.

Bergström, S.M., 1986, Biostratigraphic integration of Ordovician graptolite and conodont zones--a regional review: Geological Society, London, Special Publications Geological Society, London, Special Publications, v. 20, p. 61-78.

Bergström, S.M., 2007, The Ordovician conodont biostratigraphy in the Siljan region, south-central Sweden: a brief review of an international reference standard. in: Ebbestad, J.O.R., Wickstrom, L.M., Hogstrom, A.E.S., 2007, Field Guide and Abstracts. Estonian Geological Sections, Bulletin, vol. 7, Geological Survey of Estonia, p. 11-13.

Bergström, S.M., Chen, X., Gutiérrez‐Marco, J.C., and Dronov, A., 2009, The new chronostratigraphic classification of the Ordovician System and its relations to major regional series and stages and to $\delta^{13}C$ chemostratigraphy: Lethaia, v. 42, p. 97-107.

Berner, R.A., Petch, J.A., Lake, J.A., Beerling, D.J., Popp, B.N., Lane, R.S., Laws, E.A., Westley, M.B., Cassar, N., Woodward, F.I., and Quick, W.P., 2000, Isotope Fractionation and Atmospheric Oxygen: Implications for Phanerozoic O_2~ Evolution: Science, v. 287, p. 1630-1632.

Berner, R.A., 2004, The phanerozoic carbon cycle CO_2 and O_2: Oxford, Oxford University Press, 150 p.

Berner, R.A., VandenBrooks, J.M., and Ward, P.D., 2007, Oxygen and Evolution: Science, v. 316, p. 557-558.

Canfield, D.E., Poulton, S.W., and Narbonne, G.M., 2007, Late-Neoproterozoic Deep-Ocean Oxygenation and the Rise of Animal Life: Science, v. 315, p. 92-95.

Cocks, L.R.M., and Torsvik, T.H., 2002, Earth geography from 500 to 400 million years ago: a faunal and paleomagnetic review. Journal of the Geological Society, v. 159, p. 631-644.

Cooper, R.A., and Sadler, P.M., 2012, The Ordovician Period. in: Gradstein, F.M., Schmitz, M., and Ogg, G., The Geologic Time Scale 2012 2-Volume Set: Elsevier, p. 489-523.

Dronov, A., and Rozhnov, S.O.L., 2007, Climatic changes in the Baltoscandian basin during the Ordovician: sedimentological and palaeontological aspects: Gu Sheng Wu Xue Bao Acta Palaeontologica Sinica., v. 46, p. 108-113.

Dudley R, 1998, Atmospheric oxygen, giant Paleozoic insects and the evolution of aerial locomotor performance. The Journal of Experimental Biology, v. 201, p. 1043-50.

Graham, J.B., Dudley, R., Aguilar, N.M., and Gans, C., 1995, Implications of the late Palaeozoic oxygen pulse for physiology and evolution: Nature -London-, v. 375, p. 117.

Haq, B.U., and Schutter, S.R., 2008, A chronology of Paleozoic sea-level changes: Science, v. 322, p. 64-68.

Harris, A., Bergström, S., Ethington, R., and Ross Jr, R., 1979, Aspects of Middle and Upper Ordovician conodont biostratigraphy of carbonate facies in Nevada and southeast California and comparison with some Appalachian successions: Brigham Young University Geology Studies, v. 26, p. 7-43.

Hayes, J.M., Strauss, H., and Kaufman, A.J., 1999, The abundance of ^{13}C in marine organic matter and isotopic fractionation in the global biogeochemical cycle of carbon during the past 800 Ma: Chemical Geology, v. 161, p. 103-125.

Joachimski, M., Pancost, R., Freeman, K., Ostertag-Henning, C., and Buggisch, W., 2002, Carbon isotope geochemistry of the Frasnian–Famennian transition: Palaeogeography, Palaeoclimatology, Palaeoecology, v. 181, p. 91-109.

Kaljo, D., Martma, T., and Saadre, T., 2007, Post-Hunnebergian Ordovician carbon isotope trend in Baltoscandia, its environmental implications and some similarities with that of Nevada: Palaeogeography, Palaeoclimatology, Palaeoecology, v. 245, p. 138-155.

Krause, F., and Rowell, A.J., 1975, Distribution and systematics of the inarticulate brachiopods of the Ordovician carbonate mud mound of Meiklejohn Peak, Nevada: The Paleontological Institute, The University of Kansas. Description: 86 p.

Kump, L.R., and Arthur, M.A., 1999, Interpreting carbon-isotope excursions: carbonates and organic matter: Chemical Geology, v. 161, p. 181-198.

Kump, L., Arthur, M., Patzkowsky, M., Gibbs, M., Pinkus, D., and Sheehan, P., 1999, A weathering hypothesis for glaciation at high atmospheric pCO_2 during the Late Ordovician: Palaeogeography, Palaeoclimatology, Palaeoecology, v. 152, p. 173-187.

Mannik, P., Viira, V., 2005, Distribution of Ordovician conodonts. in: Põldvere, A. (Ed.), Mehikoorma (421) Drill Core, Estonian Geological Sections, Bulletin, vol. 6, Geological Survey of Estonia, p. 16-20.

Miller, James F., Kevin R. Evans, and Benjamin F. Dattilo, 2012, The great American carbonate bank in the miogeocline of western central Utah: Tectonic influences on sedimentation. in J. R. Derby, R. D. Fritz, S. A. Longacre, W. A. Morgan, and C. A. Sternbach, eds., The great American carbonate bank: The geology and economic resources of the Cambrian – Ordovician Sauk megasequence of Laurentia: AAPG Memoir 98, p. 769 – 854.

Monsen, S.A., Carr, M.D., Reheis, M.C., Orkild, P.P., 1992, Geologic map of Bare Mountain, Nye County, Nevada: U.S. Geological Survey, scale 1:62,500, 1 sheet.

Nielsen, A.T., 2004, Ordovician sea level changes: a Baltoscandian perspective. in: Webby, B.D., The Great Ordovician Biodiversification Event, p. 84-93.

Popp, B.N., Laws, E.A., Bidigare, R.R., Dore, J.E., Hanson, K.L., and Wakeham, S.G., 1998, Effect of phytoplankton cell geometry on carbon isotopic fractionation: Geochimica Et Cosmochimica Acta, v. 62, p. 69-77.

Ross, R.J., 1972, Fossils from the Ordovician bioherm at Meiklejohn Peak, Nevada: U.S. Geological Survey, Professional Paper: 685, 47 p.

Ross JR, R.J., James, N.P., Hintze, L.F., and Poole, F.G., 1989, Architecture and evolution of a Whiterockian (early Middle Ordovician) carbonate platform, Basin Ranges of western USA: Special Publications of SEPM.

Saltzman MR, Young SA, Kump LR, Gill BC, Lyons TW, and Runnegar B, 2011, Pulse of atmospheric oxygen during the late Cambrian. Proceedings of the National Academy of Sciences of the United States of America, v. 108, p. 3876-81.

Schmitz, B., Bergström, S.M., and Xiaofeng, W., 2010, The middle Darriwilian (Ordovician) $\delta^{13}C$ excursion (MDICE) discovered in the Yangtze Platform succession in China: implications of its first recorded occurrences outside Baltoscandia: Journal of the Geological Society, v. 167, p. 249-259.

Sepkoski, J.J., 1995, Life from the Beginning: Science, v. 268, p. 1206-1207.

Trotter J.A., Williams, I.S., Barnes, C.R., Lécuye, C., and Nicoll, R.S., 2008, Did cooling oceans trigger Ordovician biodiversification? Evidence from conodont thermometry: Science, v. 321, p. 550-554 .

Viira, V., Löfgren, A., and Sjöstrand, L., 2006, Distribution of Ordovician conodonts. in: Põldvere, A. (Ed.), Kerguta (565) Drill Core, Estonian Geological Sections, Bulletin, v. 7, Geological Survey of Estonia, p. 11-13.

Webby, B.D., 2004, The great Ordovician biodiversification event: New York, Columbia University Press.

Young, S.A., Saltzman, M.R., Foland, K.A., Linder, J.S., and Kump, L.R., 2009, A major drop in seawater $^{87}Sr/^{88}Sr$ during the Middle Ordovician (Darriwilian): Links to volcanism and climate?: Geology, v. 37, p. 951-954 .

Appendix

Table 1. Stable isotope data, Meiklejohn Peak, Nevada. No entry for "Meters" signifies a rerun of the identical sample listed directly above.

Meters	$\delta^{13}C_{carb}$	$\delta^{18}O_{carb}$	$\delta^{13}C_{org}$	$\Delta^{13}C$
0.0	-0.38	-8.65	-28.76	28.38
12.0	-0.43	-6.74	-28.91	28.48
15.0	-0.32	-6.93		
21.0	-0.15	-8.23		
27.0	-0.24	-7.36	-29.27	29.03
30.0	-0.41	-8.12		
33.0	-0.33	-7.83		
37.5	-0.40	-7.23	-29.21	28.81
40.5	-0.92	-7.24		
43.5	-0.70	-7.22		
48.0	-1.14	-7.27		
49.5	-1.12	-6.65		
52.5	-0.37	-7.18		
57.0	-0.14	-7.96	-29.04	28.90
61.5	-1.33	-8.23		
64.5	-1.57	-8.44		
67.5	-1.25	-6.87		
70.5	-1.54	-7.33		
73.5	-1.89	-7.57		
79.5	-1.75	-7.25	-29.81	28.06
79.5	-1.76	-7.27		
82.5	-2.36	-7.71		
85.5	-2.15	-7.56		
88.5	-1.93	-7.35	-29.95	28.02
91.5	-1.81	-8.14		
94.5	-1.36	-7.46		
96.0	-0.08	-7.48		
97.5	-0.21	-7.37	-29.49	29.29
99.0	-0.56	-6.98		
100.5	-0.75	-7.53		
102.0	-1.15	-8.13		
103.5	0.39	-7.37	-30.56	30.95
106.5	0.32	-6.82		
109.5	0.39	-7.49	-30.69	31.08
112.5	0.48	-7.48		
115.5	0.29	-7.45	-30.93	31.22
118.5	0.45	-7.39		
121.5	0.46	-7.53	-30.86	31.32

Meters	$\delta^{13}C_{carb}$	$\delta^{18}O_{carb}$	$\delta^{13}C_{org}$	$\Delta^{13}C$
124.5	-0.89	-6.77		
129.0	0.25	-6.88	-30.19	30.44
	0.29	-6.70		
130.5	-0.21	-7.09		
135	-0.51	-6.46	-30.15	29.65
138.0	-0.07	-6.98		
142.5	0.79	-6.58	-30.39	31.18
148.5	0.26	-6.44	-31.01	31.27
153.0	-0.25	-6.90	-28.71	28.45
159.0	0.32	-6.17	-29.67	29.99
166.5	0.47	-11.04	-29.73	30.20
174.0	0.28	-6.31	-31.15	31.43
180.0	0.07	-6.52	-30.07	30.15
186.0	0.42	-7.48	-29.88	30.29
	0.49	-7.35		
193.5	0.36	-6.46	-28.66	29.02
201.0	0.70	-6.52	-29.77	30.47
207.0	0.17	-6.65		
	0.02	-6.60		
214.5	0.46	-6.06	-30.19	30.66
216.0	-0.67	-6.83		
217.5	0.28	-6.32		
219.0	-0.07	-1.97		
220.5	0.63	-6.09	-29.69	30.33
222.0	0.59	-10.15		
225.0	-1.26	-10.36		
226.5	0.14	-7.05		
228.0	-0.10	-8.66	-29.55	29.46
231.0	-0.34	-6.81	-29.87	29.53
232.5	-0.59	-6.56		
234.0	0.26	-14.58	-29.93	30.19
	0.26	-8.19	-29.90	30.16
235.5			-30.97	
237.0	0.15	-6.63		
238.5	-0.07	-10.76		
240.0	0.47	-5.92	-29.78	30.26
243.0	-1.23	-6.95	-30.93	29.70
247.5	-1.30	-5.93	-31.67	30.37
250.5	-1.82	-8.15	-29.69	27.87
252.0	-2.10	-7.63	-29.88	27.78
253.5	-1.72	-4.82		
258.0	-2.29	-8.65	-27.79	25.50

Meters	$\delta^{13}C_{carb}$	$\delta^{18}O_{carb}$	$\delta^{13}C_{org}$	$\Delta^{13}C$
259.5	-1.55	-6.82		
261.0	-1.92	-8.18	-28.18	26.26
			-28.10	
264.0	-2.10	-8.29	-28.32	26.22
264.0	-2.17	-10.50		
269.0	-2.73	-10.05	-27.68	24.95
270.0	-2.29	-8.80	-28.46	26.17
	-1.96	-7.50		